Study on Morphology Development for *In situ* Fiber–Reinforced Composites by Blending Polyolefin and Polycaprolactone

Takeshi Semba,[1] Kazuo Kitagawa,[1] Masahiko Nakagawa,[2] Umaru Semo Ishiaku,[3] Hiroyuki Hamada[3]

[1]*Department of Applied Chemistry, Kyoto Municipal Industrial Research Institute Industrial Research Center, 134, Chudoji Minami-machi, Shimogyo-ku, Kyoto, 600-8813, Japan*
[2]*Technology and Development Department, Hexa Chemical Co., Ltd., 153, Yokomakura-Nishi, Higashi-Osaka-City, 578-0956, Japan*
[3]*Division of Advanced Fibro-science Kyoto Institute of Technology, Gosyokaido-cho, Matsugasaki, Sakyo-ku, Kyoto, 606-8585, Japan*

Received 22 July 2004; accepted 4 January 2005
DOI 10.1002/app.22137
Published online in Wiley InterScience (www.interscience.wiley.com).

ABSTRACT: The morphology developments and interfacial properties of extruded polyethylene/polycaprolactone and polypropylene/polycaprolactone blends were investigated. The interfacial thicknesses of both polymer blends were thin and this was investigated by interfacial tension measurement in the melt state. The aspect of boundary area was observed by AFM, and a clear line could be observed at the interface area as a result of thin interfacial thickness. The *in situ* fiber formation of the dispersed phase was remarkably generated under elongational flow (between die exit and solidification) rather than under shear flow (in the cylinder and die). Drawing ratio was varied at three levels to study its effect on elongation of the dispersed phases. The dispersions dramatically changed from spherical to spheroidal and filament shapes depending on the drawing ratio. Reduced capillary number (Ca*) was used to characterize droplet deformation. The deformation mode under shear flow was classified as nondeformation mode due to the fact that the Ca* was almost 0. On the other hand, the deformation mode under elongational flow was classified into filament shape mode (Ca* > 4). This classification was in agreement with the SEM images. The tensile properties were increased at the border line where the Ca* was 4.0. The melt interfacial tensions of polyolefin/polycaprolactone were relatively large, and a clear line could be observed at the interface area as a result of little affinity of polymer interface.
 J Appl Polym Sci 98: 500–508, 2005

Key words: blending; composites; fibers; morphology; polypropylene

INTRODUCTION

Morphology control in polymer blend materials is a key technique to create functional and toughened composites. The morphologies are changed to various shapes, such as spherical, spheroid, lamella, and filament, to obtain different properties, e.g., microrubber particles dimensions affect impact strength, and a special gas barrier property is brought about by the lamella structure.[1–3] These high performance polymer blend materials are valuable for practical use. The authors have been researching a polymer blend that has long fibers as a dispersed phase to reinforce the polyolefin matrix.[4–7] Low-density polyethylene (LDPE) and high-density polyethylene (HDPE) matrices is effectively reinforced by polyester resin with the latter dispersed as long fibers.[8] This composite has good static and dynamic mechanical properties as well. In the case of the polypropylene (PP)/polycaprolactone (PCL) blend sheets fabricated by extrusion,[7] the combined effect of shear and elongational flows during processing prompted the dispersed phase to transform into long fiber reinforcements. The *in situ* fiber reinforcement results in synergism in tensile strength and tensile modulus, and the crystallinity of the dispersions is higher than that of spherical dispersions.

The final morphology in polymer blends depends on many conditions, such as viscosity ratio, interfacial tension of polymer materials, flow fields, and cooling speed of moldings. Taylor[9,10] reported on the morphology of emulsions consisting of two fluids in various flow fields at the beginning of the 1930s. They found that there is a relationship between viscosity ratio and droplet deformation. Later, many researchers investigated the deformation mechanism of dispersed polymer droplets. Lately, Huneault et al.[11] and Song et al.[12] have predicted dispersed morphology and size of a polymer blend by simulation.

The dispersed PCL is easily deformed into long fibers under extrusion and could effectively reinforce

Correspondence to: T. Semba (sentake@city.kyoto.jp).

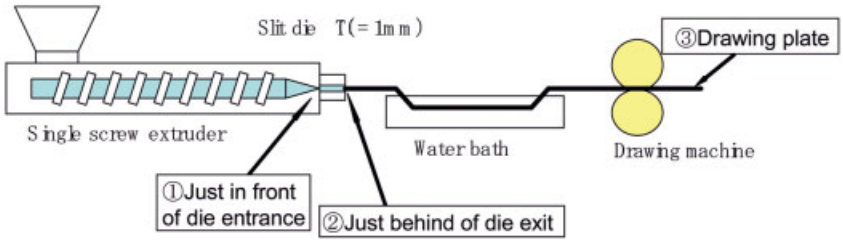

Figure 1 Observation parts in extrusion process. 1, Just in front of die entrance; 2, just behind die exit without drawing; 3, drawing plate. [Color figure can be viewed in the online issue, which is available at www.interscience.wiley.com.]

the polyolefin matrix. The verification of morphological development provided much beneficial information about assembled polymer blend materials and was used in fixing optimum processing conditions. The aim of this study is to clarify the mechanism of *in situ* fiber formation in a polyolefin/polycaprolactone (PCL) blend during extrusion. The interfacial properties of the polymer blend were evaluated by using interfacial tension measurement and magnification imaging by using atomic force microscopy (AFM). The deformation types of dispersed droplets were classified into three modes, e.g., nondeformation, breakup, and fiber formation. The relationships between the deformation mode and the mechanical properties were verified. A capillary number (Ca) was introduced by the authors to classify deformation mode.[9–12] The relationship between morphology and extent of elongation was investigated by changing the drawing ratio at three levels.

EXPERIMENTAL

Material and compounding

The materials used in this study were homo-polypropylene (PP) (IDEMITSU PP, J900GP, melt index = 13 g/10 min; Idemitsu Petrochemical Co., Ltd), LDPE (Petrosen349, melt index = 13 g/10 min; Tosoh Corp.), and polycaprolactone (Cel green PH7, melt index = 2.3 g/10 min; Daicel Chemical Industries, Ltd.).

Shear rate dependence of viscosity at high shear rate area ($> 100\ s^{-1}$) was measured by using a capillary type rheometer (Capirograph IB; Toyo Seiki Seisaku-sho, Ltd.). Bagley end correction and Rabinovitsch correction methods were employed to calculate real viscosities with correct shear stress and shear rate data. Three capillary dies (L/D = 10, 20, and 40, diameter = 1.0 mm) were used. The rheometer of parallel plate type discs (ARES; Rheometric Scientific F.E. Ltd.) provided the shear rate dependence of viscosity at low shear rate area ($0.01 \sim 100\ s^{-1}$) based on time–temperature superposition. Both viscosity data measured by capillary and plate type discs were superposed according to Cox–Merz empirical law.[13]

The blend ratio of polyolefin/PCL was 8/2 by weight. A single-screw extruder (PSV30: Pula Enge Co., Ltd. L/D = 32) equipped with slit type die was employed for compounding and fabricating blend sheets (see Figure 1). The processing temperature was 200°C at the die area. The drawing speed behind the slit die was varied by three steps from 1.0 to 3.4 as shown in Table I, where the 1.0 indicates that cross section of a sheet sample is equal to the die slit in area.

Evaluation of polymer interface

The melt interfacial tension data is important data because polymer mixing is carried out in the molten state. The melt interfacial tension of PP/PCL and LDPE/PCL were measured by using sessile and pendant drop methods.[14,15] To calculate the polarity ratio of polymer solids, PP, LDPE, and PCL films with flat surfaces were prepared with a hot press machine (NF-50 Shinto Metal Industries Ltd.). Three kinds of liquids [distilled water as polar liquid, ethylene glycol as neutral polar liquid, and diiodomethane as nonpolar liquid (see Table II)] were dropped onto these films at room temperature. The contact angles were obtained from video images and then used to calculate surface tension by applying the geometric-mean method of the Owence, Wendt, Rabel, and Kaelble equation.[16,17]

$$\gamma_{sl} = \gamma_{lv} + \gamma_{sv} - 2\sqrt{\gamma_{lv}^{d} \times \gamma_{sv}^{d}} - 2\sqrt{\gamma_{lv}^{p} \times \gamma_{sv}^{p}} \qquad (1)$$

They combined the Young equation, $\gamma_{sl} = \gamma_{sv} - \gamma_{lv} \times \cos\theta$ and eq. (1), and the resulting equation is shown below:

TABLE I
Drawing ratio of Polyolefin/PCL Blends

	Drawing ratio (−)		
Combination	A	B	C
PP/PCL	1.0	1.6	3.3
LDPE/PCL	1.0	2.0	3.4

TABLE II
Surface Tensions and Densities Data of Liquids Used for Sessile Drop Test

Liquid	γ_{lv}	γ_{lv}^{d} (mN/m)	γ_{lv}^{p}	Density (g/cm3)
Distilled water	72.8	21.8	51.0	0.998
Ethylene glycol	47.7	30.9	16.8	1.11
Diiodemethane	50.8	48.5	2.30	3.33

$$\sqrt{\gamma_{sv}{}^{p}} \times \sqrt{(\gamma_{lv}{}^{p}/\gamma_{lv}{}^{d})} + \sqrt{\gamma_{sv}{}^{d}} = [(1 + \cos\theta) \times \gamma_{lv}]/2\sqrt{\gamma_{lv}{}^{d}} \quad (2)$$

where the γ is interfacial tension and the subscripts s, l, and v correspond to solid, liquid, and vapor, respectively, while θ is the contact angle. The subscripts p and d refer to polar and the dispersed parts of surface tension.

The γ_{sv}^{p} is obtained from the square of the slope of the line, and the γ_{sv}^{d} is obtained from the square of the ordinate intercept.

The polarity ratio is expressed as follows:

$$\chi = \gamma_{sv}^{p}/(\gamma_{sv}^{d} + \gamma_{sv}^{p}) \quad (3)$$

The polarity ratio, which is independent of temperature, is applicable for surface tension of polymer melts.[14]

To determine the total surface tension of polymer melts, pendant drops of polymer melts were formed in a chamber at 200°C. This chamber was filled with nitrogen gas to prevent oxidation. The hydromechanical equilibrium of the pendant drop is described by the classical Laplace equation:[18,19]

$$\gamma(1/R_1 + 1/R_2) = \Delta P \quad (4)$$

where γ is the interfacial tension, R_1 and R_2 are two principle radii of curvature, and ΔP is the pressure difference between the outside and the inside of the drop. The surface tension of polymer melts was taken as the average of constant pendant drop contour.

The density of polymer melt was measured by using PVT apparatus at a temperature of 200°C and pressure change from 5 to 100 MPa. The pressure in the cylinder, die, and sheeting process was assumed to be atmospheric pressure. The density of polymer melt at atmospheric pressure was an extrapolated value calculated by the data from 5 to 100 MPa. Interfacial tension of polymer melts was calculated from Wu's harmonic-mean equation:[14]

$$\gamma_{12} = \gamma_1 + \gamma_2 - [4\gamma_1^{d}\gamma_2^{d}/(\gamma_1^{d} + \gamma_2^{d})] - [4\gamma_1^{p}\gamma_2^{p}/(\gamma_1^{p} + \gamma_2^{p})] \quad (5)$$

where the subscripts 1 and 2 denote phase1 and phase 2, respectively. This equation is the most applicable for interfacial tension of polymer melts.

The interfacial area between the polyolefin and the PCL phase was directly observed by using AFM (Nanoscope IIIa; Digital instruments Co., Ltd.). The cross-sectional area along the flow direction was adjusted with a flat surface by using a microtome (HM30; Microm International GmbH) equipped with a glass knife. The tapping mode of the most common observation method in AFM was applied to the cross-sectional area, and the phase images were taken.

Observation of dispersed phase

To classify the deformation mode during extrusion, the shape and size of droplets were measured at the following positions, 1, just in front of the die entrance, 2, behind the die exit without drawing, 3, after drawing into a plate (see Figure 1). Screw mixing of all polymers is completed at position 1, while shear deformation would occur from positions 1 to 2, and elongational deformation would cause the deformation of dispersed phase from positions 2 to 3. The observation of morphology was done with a scanning electron microscope (SEM) (JSM5900LV; JEOL Ltd.). The PCL dispersions of the blend sheets were extracted using chloroform in a Soxhlet extractor. The voids in the photograph were traced and converted to binary images. The droplet length (FD-l), width (TD-w), and volume average radius (R_v) were calculated (see Figure 2). The effective capillary number (Ca) can be calculated using:

$$\mathrm{Ca} = \tau \times R/\sigma = \eta_m \times \gamma \times R/\sigma \quad (6)$$

where τ is the hydrodynamic stress such as shear and elongational stress, R is the radius of the droplet, σ is the interfacial tension, η_m is the viscosity of the matrix, γ is the shear rate or the deformation ratio in the elongational flow process. The Ca has a critical value ($\mathrm{Ca_c}$) whereby the droplets are not deformed and maintain a regular shape. The $\mathrm{Ca_c}$ only depends on the viscosity ratio ρ:

$$\rho = \eta_d/\eta_m \quad (7)$$

where η_d and η_m are the viscosity of dispersed and matrix polymers, respectively. The minimum $\mathrm{Ca_c}$ value is achieved at $\rho = 1.0$.[11,12] The $\mathrm{Ca_c}$ values show different behaviors under shear and elongational flows.[9,11,18] Under shear flow, the $\mathrm{Ca_c}$ is infinity when the ρ exceeds 3.8. On the other hand, the $\mathrm{Ca_c}$ value is less than 1.0 throughout a broad range ($10^{-5} < \rho < 10^{3}$) in the elongational flow field. The reduced capillary number (Ca*) expressed in eq. (8) describes the deformation mode:

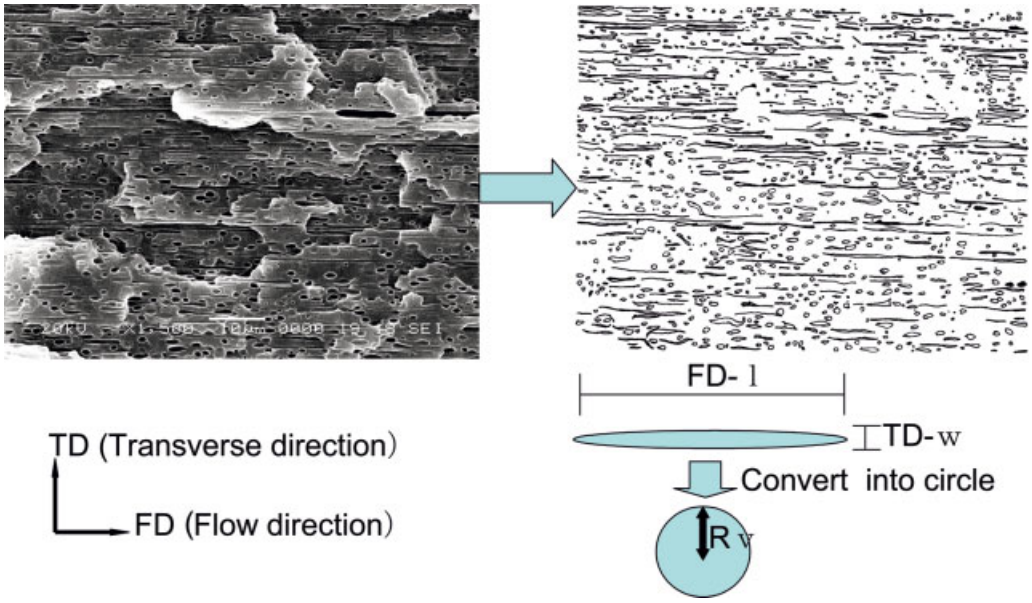

Figure 2 Converted binary image and measurements of droplets. [Color figure can be viewed in the online issue, which is available at www.interscience.wiley.com.]

$$Ca^* = Ca/Ca_c \quad (8)$$

The deformation modes of dispersed droplets are classified as follows: (a) $Ca^* < 0.1$ signifies nondeformation, (b) $0.1 < Ca^* < 1$ signifies deformation, (c) $1 < Ca^* < 4$ signifies break up, and (d) $4 < Ca^*$ signifies deformation into fiber shape.

Mechanical properties

A tensile test of the blend sheets along the flow direction was performed with a universal testing machine (Autograph AG-5000E; Shimadzu, Corp.) at a crosshead speed of 5 mm/min at room temperature. The gauge length was 65 mm.

RESULTS AND DISCUSSION

Interfacial properties

Melt interfacial tension data is important because polymer mixing is carried out in the molten state. The melt interfacial tension of PP/PCL and LDPE/PCL were measured by using sessile and pendant drop methods as discussed above. Contact angle and surface tension results of polymer solids from measuring the sessile drop are listed in Table III. The contact angles of PP and LDPE were almost the same for all liquids. PCL showed a low contact angle value in contrast to polyolefin resins. The surface tension of polyolefin materials had no polarity as they contained only the dispersed (nonpolar) components. On the other hand, PCL is polar, and the polarity ratio (χ_p) was 0.2. The polarity ratio, which is independent of temperature, is applicable for the surface tension of polymer melts. Table IV shows the interfacial tension of polyolefin/PCL at 200°C. The interfacial tensions of both polymer combinations were close to each other. There are some polymer combinations of the same interfacial tension level, for example, the PE/PS (5.8 mN/m at 180°C), PP/PS(5.1 mN/m at 140°C), and PET/EPR (6.2 mN/m at 280°C).[20] It has been shown that *in situ* fiber formation of the PP/PS blend occurred during polymer processing. It is thought that there is a possibility of fiber formation in these materials, when other conditions (e.g., viscosity ratio, hydrodynamic stress, etc.) are suitable. The interfacial tension is related to interfacial thickness; in other words, the interfacial tension would be inversely proportional to the interfacial thickness. The equation for the relation between the interfacial tension and interfacial thickness is as follows:

TABLE III
Contact Angle and Surface Tension Results from Measurement of Sessile Drop

	Matrix		Dispersion
	PP	LDPE	PCL
Contact angle(°)			
Distilled water	104	105	74.3
Ethylene glycol	78.7	81.5	61.4
Diiodemethane	55.6	55.5	36.0
Surface tension(mN/m)			
γ_{sv}	29.1	28.8	36.3
γ_{sv}^d	29.0	28.8	29.1
γ_{sv}^p	0	0	7.22
χ_p	0	0	0.2

TABLE IV
Interfacial Properties of Polyolefin/PCL at 200°C

	Matrix		Dispersion
	PP	LDPE	PCL
Density (g/cm^3)	0.753	0.763	0.934
γ_{sv} (mN/m)	18.8	19.2	27.8
Interfacial tension against PCL (mN/m)	5.85	5.66	—
Interfacial thickness (nm)	1.36	1.41	—

$$\gamma = 7.6L^{-0.86} \quad (9)$$

where γ is interfacial tension and L is interfacial thickness.[14] The calculated interfacial thicknesses of PP/PCL and LDPE/PCL were only 1.36 and 1.41 nm, respectively (see Table IV). The interfacial thickness of polymer blends have been reported (e.g., the thickness of a partial compatible polymer blend as PC/SAN is about 4 nm, that of a compatible polymer blend as SBR/BR is larger than 20 nm, furthermore, that of the polyamide/SAN with SMA of interfacial activator is about 50 nm).[21,22] It was clearly indicated that the interfacial thickness of both polyolefin/PCL blends were thin, contrary to that of compatible polymer blends.

Accordingly, AFM observation of the interfacial area of $\gamma = 1.0$ drawn sheets was carried out without extraction of PCL. The flattened samples were obtained using a microtome. AFM images of PP/PCL are shown in Figure 3. These photographs were captured in the phase imaging mode in which the image contrast describes the stiffness and viscoelasticity of the materials. The dark area is the PCL phase, while the PP is the bright area. The PCL component was formed as fibrous and spherical inclusions in the PP matrix. The width of fiber was about 400 nm, but the length was to great to be determined. A clear line, which shows thin interfacial thickness, could be seen at the interfacial area in the high magnification photograph. It is obvious that there is no boundary layer that can be seen in the incompatible polymer blend. The interfacial area of LDPE/PCL was almost the same as that of PP/PCL as shown in Figure 4. For example, the AFM images of PLA (polylactic acid)/PCL blend film, which is a more compatible polymer blend (interfacial tension is 0.32 mN/m at room temperature) in contrast with polyolefin/PCL, are shown in Figure 5.[23] The blurred boundary area in which the molecules of both phases interpenetrated can be observed in the high magnification image, and the interfacial thickness was about 10–21 nm. It is obvious that the interfacial area of polyolefin/PCL with high interfacial tension is different from lower interfacial tension blends.

Morphological transition in the slit die

Shear rate dependence of viscosity for each of the materials are shown in Figure 6. Smooth curves could be drawn owing to the superposition of the data from capillary and plate type rheometers. The viscosity of PCL was the highest of the three materials at all shear rate regions. The viscosity of the PP was higher than that of LDPE at low shear rate, but this was inverted at high shear rate. The viscosities were identical at the shaded area, which signifies the shear rate in the slit die. The shear rate in the slit die was calculated as:

$$\gamma = 6Q/WH^2 \quad (10)$$

where Q is the extruded volume per unit time, W is the width of the slit die, and H is the thickness of the slit

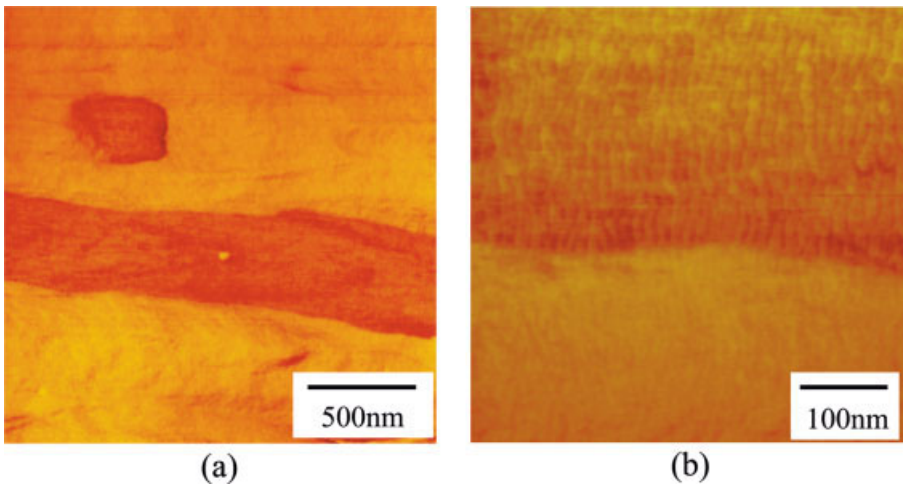

Figure 3 AFM image of the interfacial area of PP/PCL blend ($\gamma = 1.0$). (a) Low magnification; (b) high magnification. [Color figure can be viewed in the online issue, which is available at www.interscience.wiley.com.]

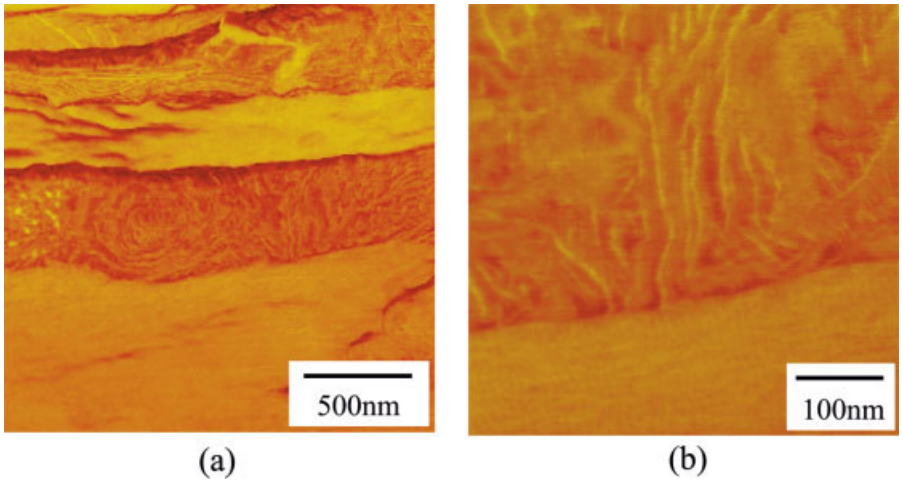

Figure 4 AFM image of the interfacial area of LDPE/PCL blend (γ = 1.0). (a) Low magnification; (b) high magnification. [Color figure can be viewed in the online issue, which is available at www.interscience.wiley.com.]

die. The zero shear viscosity of each material was observed at low shear rates.

Figure 7 shows the morphology transition in PP/PCL and LDPE/PCL blends from position 1 to 2 (see Figure 2). The value of R_v for both samples increased after passing through the slit die, while the values of TD-w were almost the same. If droplet deformation actually occurred, then TD-w of 2 must be smaller than that of 1. These results show the occurrence of coalescing droplets, and the deformation of droplets was minimal in the slit die. Here, the Ca* under shear flow were calculated by eq. (8) to classify the deformation mode. The viscosity ratios, ρ, of PP/PCL and LDPE/PCL were 6.4 and 6.5. The value of capillary number Ca* for both blends is almost 0 since the critical value ($Ca_{c)}$ was close to infinity. In the case of $\rho > 3.8$, the value of Ca_c becomes infinity during shear flow. This means the deformation mode is that of (a) Ca* < 0.1, i.e., nondeformation. To generate fiber reinforcements, a higher viscosity matrix in the shear flow would be necessary.

Figure 8 shows the morphological transition of both blends with three stages of drawing ranging from 1.0 to 3.4. In the case of PP/PCL blend, the dispersed shape of drawing ratio 1.0 was obviously different from that of 1.6. When the drawing ratio is 1.0, small spherical droplets, which have an R_v of 0.62 μm and a TD-w of 0.57 μm, were generated due to break up of the dispersed phase, and Ca* value was 3.1, which conforms to the deformation mode of (c) $1 <$ Ca* < 4, i.e., break up. Here, the elongational viscosity was calculated as three times the zero shear viscosity, and γ was the deformation ratio of the cross-sectional area of the blend sheet divided that of the slit die. The samples drawn at 1.6 and 3.3 ratio had notably long dispersed fibers. This morphology is easily distinguishable from that in which the drawing ratio is

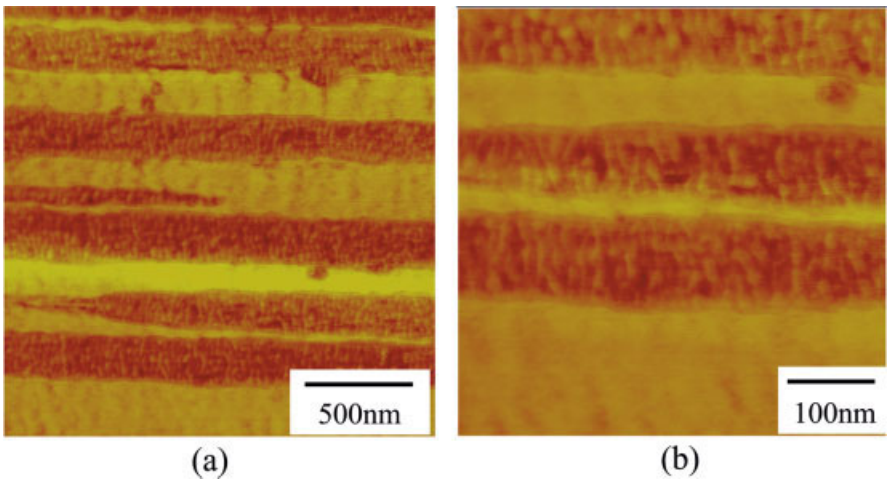

Figure 5 AFM image of the interfacial area of PLA/PCL blend. (a) Low magnification; (b) high magnification. [Color figure can be viewed in the online issue, which is available at www.interscience.wiley.com.]

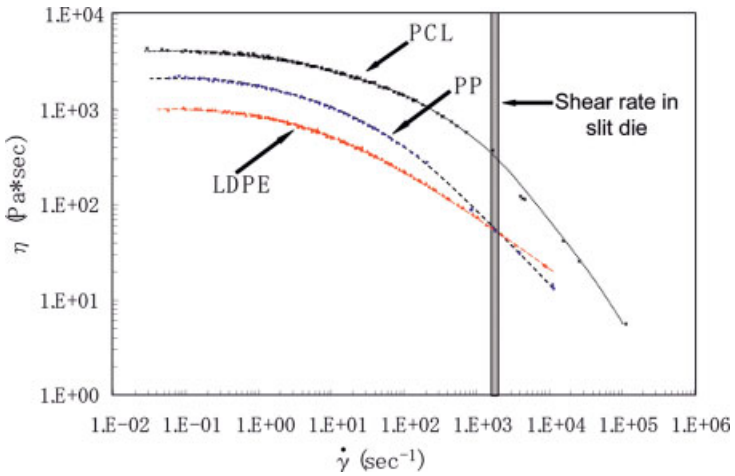

Figure 6 Relationship between viscosity and shear rate of each material. [Color figure can be viewed in the online issue, which is available at www.interscience.wiley.com.]

1.0. The average fiber length could not be measured from these photographs, therefore the inferential length was calculated from the average radius of fibers (TD-w) by observing the cross section of the transverse direction (see Figure 9), where the R_v was assumed to be 1.19 μm at position 2. This measurement was based on the inference that there is no coalescence and break up of droplets from positions 2 to 3. These fiber lengths were 56.4 and 133 μm, respectively. These fiber lengths are illustrated on the Figure 8. The TD-w with a drawing ratio of 3.3 was smaller than that with a drawing ratio of 1.6; the elongation degree of droplets at position 2 depend on the drawing ratio. The samples drawn with 1.6 and 3.3 ratios were classified as the deformation mode of (d) 4 < Ca*, fiber shape.

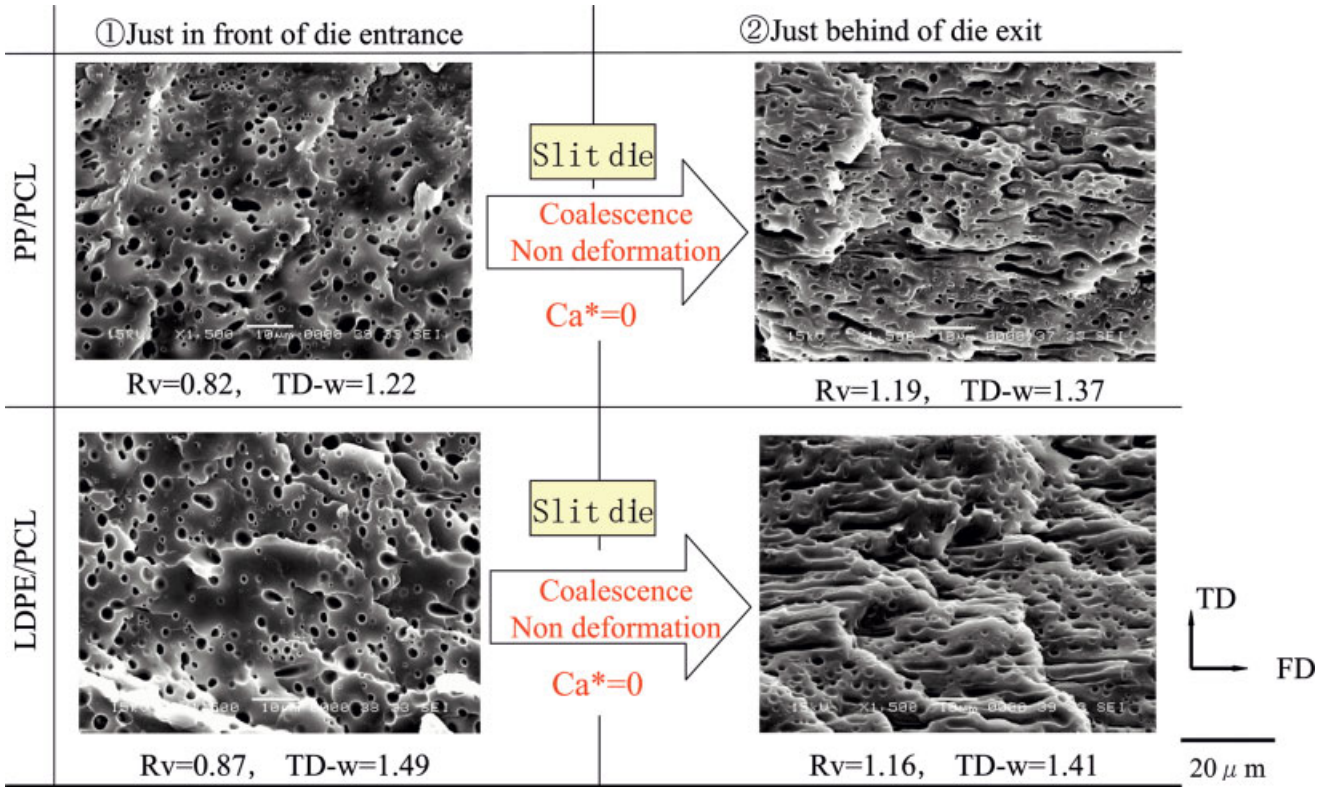

Figure 7 Morphology transition from position 1 to 2. [Color figure can be viewed in the online issue, which is available at www.interscience.wiley.com.]

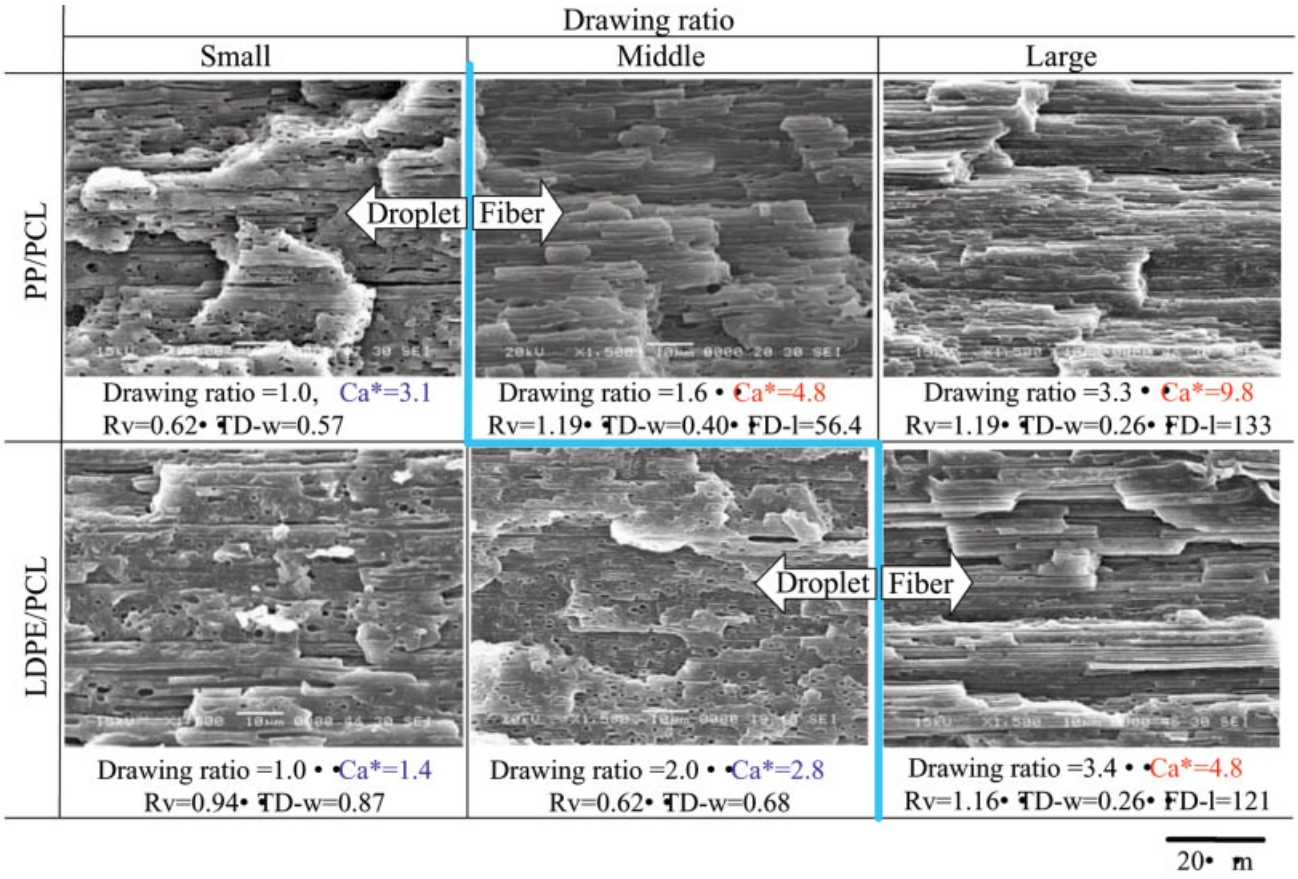

Figure 8 Morphology transition with various drawing ratios. [Color figure can be viewed in the online issue, which is available at www.interscience.wiley.com.]

The morphological transitions of the LDPE/PCL blend with various drawing ratios were a little different from that of the PP/PCL blend. The samples with 1.0 and 2.0 drawing ratios belong to the deformation mode of values (c) $1 < Ca^* < 4$, i.e., break up. The R_v and TD-w values decreased with the increasing drawing ratio, signifying the break up of the droplets. On the other hand, fine fibers were generated at 3.4 drawing ratio. The inferential fiber length was 120 μm, and the Ca* was 4.8, which can be classified as the deformation mode of (d) $4 < Ca^*$, i.e., fiber shape. Thus, it can be observed that the fiber formation of droplets in the PP/PCL blend was easier than that in LDPE/PCL blend in the elongational flow process. For the sake of further fiber formation in the LDPE/PCL blend, the

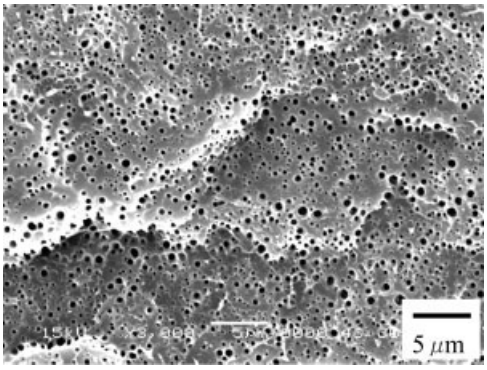

Figure 9 Cross-sectional area of transverse direction for measuring TD-w of fibers.

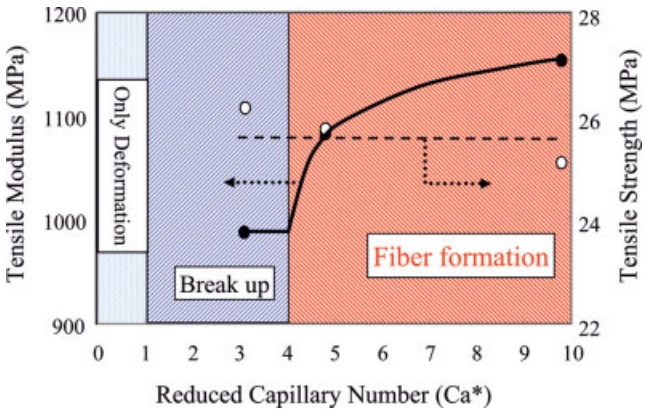

Figure 10 Relationship between tensile properties and reduced capillary number of PP/PCL blend. [Color figure can be viewed in the online issue, which is available at www.interscience.wiley.com.]

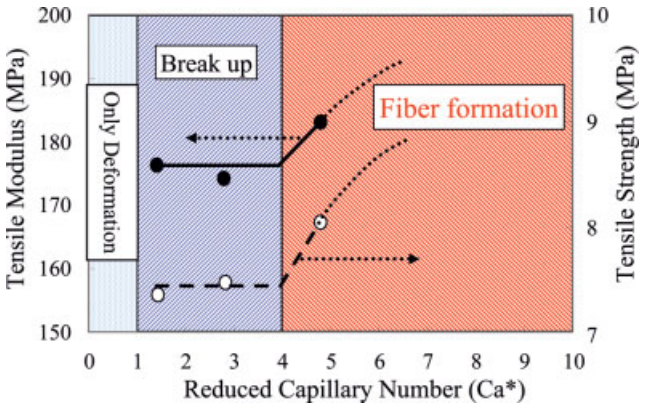

Figure 11 Relationship between tensile properties and reduced capillary number of LDPE/PCL blend. [Color figure can be viewed in the online issue, which is available at www.interscience.wiley.com.]

elongational viscosity ratio ρ should be close to 1.0. This can be done by blending a PE with a higher elongational viscosity.

Mechanical properties

Figures 10 and 11 show the relationship between tensile properties along the flow direction and Ca*. The deformation modes, i.e., break up and fiber formation, are illustrated in these figures. The tensile properties of both blends were constant until Ca* < 4. But only that of PP/PCL blend was notably increased after the line divided at Ca* $= 4$ and continued to increase until it reached a plateau area of fiber formation mode. The mechanical properties of the LDPE/PCL blend after Ca* > 5 were anticipated as an extrapolation. It is obvious that the tensile properties strongly depend on fiber formation. Tensile modulus follows a similar trend in both blends by showing continuous increase beyond Ca* $= 4$.

CONCLUSIONS

1. The interfacial tension of PP/PCL and LDPE/PCL were close to each other, and the interfacial thickness that is inversely proportional to the interfacial tension was thin in contrast to the more compatible polymer blends.
2. Fiber formation was dominated by the elongational flow rather than the shear flow.
3. In the case of shear flow in the die, the coalescence of droplets occurred, which implies that the polyolefin matrices would need higher viscosity for fiber formation to occur.
4. In the case of elongational flow during the drawing process, the droplets were extended conspicuously. The degree of elongation was dependent on the drawing ratio.
5. The tensile properties were in agreement with the condition of fiber formation whereby the Ca* is larger than 4.0. The morphology and mechanical properties of *in situ* fiber–reinforced composites could be predicted by using the reduced capillary number (Ca*).

References

1. Chiu, D. S.; Zhang, Z.; Siu, G. G. J Reinforced Plast Compos 1996, 15, 74.
2. Subramanian, P. M. Society of Plastics Engineers. 51st Annual Technical Conference, New Orleans, LA, 1993; p 2463.
3. Subramanian, P. M. Polym Eng Sci 1985, 25, 483.
4. Semba, T.; Kitagawa, K.; Hamada, H. The 6th Japan International SAMPE Symposium, Tokyo, Japan, 1999, 2, 921.
5. Semba, T.; Kitagawa, K.; Hamada, H. 3rd Joint Canada–Japan Workshop on Composites, Kyoto, Japan, 2000; p 395.
6. Semba, T.; Kitagawa, K.; Hamada, H. Society of Plastic Engineers, Annual Technical Conference, Chicago, IL, 2004; p 2966.
7. Semba, T.; Kitagawa, K.; Hamada, H. J Appl Polym Sci 2004, 91, 833.
8. Kitagawa K., Semba T., and Hamada H., J Material Sci Japan 1998, 47, 1270.
9. Taylor, G. I. Proc R Soc 1932, A138, 41.
10. Taylor, G. I. Proc R Soc 1934, A146, 501.
11. Huneault, M. A.; Shi, Z. H.; Utracki, L. A. Polym Eng Sci 1995, 35, 115.
12. Song, C. H.; Isayev, A. I. Polymer 2001, 42, 2611.
13. Cox, W. P.; Merz, E. H. J Polym Sci 1958, 18, 619.
14. Wu, S. Polymer Interface and Adhesion; Marcel Dekker: New York, 1982.
15. Wu, S. Polym Eng Sci 1987, 27, 335.
16. Owence, D. K.; Wendt, R. C. J Appl Polym Sci 1969, 13, 1741.
17. Rabel, W. Farbe+Lack 1971, 77, 997.
18. Grace, H. P. Chem Eng Commun 1982, 14, 225.
19. Rotenberg, Y.; Boruvka, L.; Neumann, A. W. J Colloid Interface Sci 1983, 93, 1.
20. Ide, F. Polym Dig 2003, 55, 6.
21. Akiyama, S.; Inoue, T.; Nishi, T.; Polymer Blend; CMC Publishing Co., Ltd.: Tokyo, Japan, 1981.
22. Ide, F. Polymer Alloy Sekkei; Kogyo Tyousakai Publishing Co., Ltd.: Tokyo, Japan, 1996.
23. Semba, T.; Kitagawa, K.; Hamada, H. The Japan Society of Polymer Processing 15th Annual Meeting, Tokyo, Japan, 2004; p 481.